



Integration of silicon-via electrodes with different recording characteristics on a glass microprobe using a glass reflowing process

Yu-Tao Lee^a, Shih-Rung Yeh^b, Yen-Chung Chang^b, Weileun Fang^{a,c,*}

^a Institute of NanoEngineering and MicroSystems, National Tsing Hua University, Hsinchu, Taiwan

^b Institute of Molecular Medicine, National Tsing Hua University, Hsinchu, Taiwan

^c Department of Power Mechanical Engineering, National Tsing Hua University, Hsinchu, Taiwan

ARTICLE INFO

Article history:

Received 11 April 2011

Received in revised form 18 May 2011

Accepted 25 May 2011

Available online 2 June 2011

Keywords:

Microprobe
Silicon electrode
Glass reflow
Back-side electrode
Double-side electrode
Sidewall electrode

ABSTRACT

Electrodes on planar type microelectromechanical system (MEMS) microprobes mainly record neurons on the top-side of probe shaft (called a top-side electrode). However, it is often necessary to record neurons other than those on the top-side of the probe shaft. This study uses the glass reflowing technique to embed silicon-vias in a glass probe to implement a microprobe capable of recording neurons around the shaft. The proposed technology makes it possible to fabricate, distribute, and integrate four types of electrodes on the shaft: top-side, back-side, double-side, and sidewall electrodes. These electrodes have different recording characteristics. The in vitro and in vivo (using crayfish and rat brain) experiments in this study shows that the top-side and back-side electrodes are respectively more sensitive to neurons on the top-side and back-side of the probe shaft. In contrast, signals recorded by double-side electrode and sidewall electrode are equally sensitive to neurons around the probe shaft. This study enables the implementation and integration of these four types of electrodes, meeting the requirements of various neural applications.

© 2011 Elsevier B.V. All rights reserved.

1. Introduction

Brain research and neuroprosthetics have advanced significantly due to the recent development of microprobes or microelectrodes. Researchers can use microprobes to stimulate neurons and record the neural activity of the brain. Researchers have thoroughly investigated microprobes fabricated by microelectromechanical systems (MEMS) technology in recent years. The most important benefit of MEMS microprobe technology is that large numbers of electrodes can be defined on small microprobe chips with precise control of electrode size and distance between electrodes (Bhandari et al., 2008, 2009; Blanche et al., 2005; Campbell et al., 1991; Herwik et al., 2009; Norlin et al., 2002). High recording density is an important criteria in effective neuroprosthetics (Nicollelis and Lebedev, 2009; Velliste et al., 2008). Precise control of electrode position can help reveal the interaction between neurons (Bartho et al., 2004; Du et al., 2009a). Thus, MEMS microprobes exhibit promising characteristics for neural applications in the future.

Microprobes can be classified as planar type and microwire type electrodes according to the probe structure and electrode arrangement (Fig. 1a and b). Most MEMS microprobes are planar type electrodes, and have a planar shaft to support electrodes. The shaft has two sides: the top-side and back-side. A metal film is typically deposited and patterned on one side of the probe shaft for planar type MEMS microprobes (called top-side electrodes in this study). On the other hand, a microwire electrode has an insulated metal shaft with an open to reveal the metal electrode at the tip of the shaft (Keefer et al., 2008; McCreery et al., 2006; Musallam et al., 2007). Unlike a planar type MEMS microprobe, a microwire electrode has a three-dimensional recording surface around the tip of shaft.

Neurons generate electrical signals (action potentials) that create an extracellular potential around the cell (Rall, 1962). Previous computational models show that the presence of a planar microprobe shaft in the brain tissue distorts this extracellular potential (Drake et al., 1988; Moffitt and McIntyre, 2005). Specifically, the extracellular potential is enhanced at the shaft surface facing the neuron, while the extracellular potential is attenuated at the other shaft surface. For a planar type MEMS microprobe, this distortion effect will limit the top-side electrode shown in Fig. 1a to recording neurons at the top-side of shaft (Drake et al., 1988; Du et al., 2009a; Moffitt and McIntyre, 2005). This phenomena also has been demonstrated in an in vivo experiment (Du et al., 2009a). The shaft of a microwire electrode also distorts the extra-

* Corresponding author at: R532, Department of Power Mechanical Engineering, No 101, Section 2, Kuang Fu Road, Hsinchu, Taiwan 30013. Tel.: +886 3 574 2923; fax: +886 3 573 9372.

E-mail address: fang@pme.nthu.edu.tw (W. Fang).

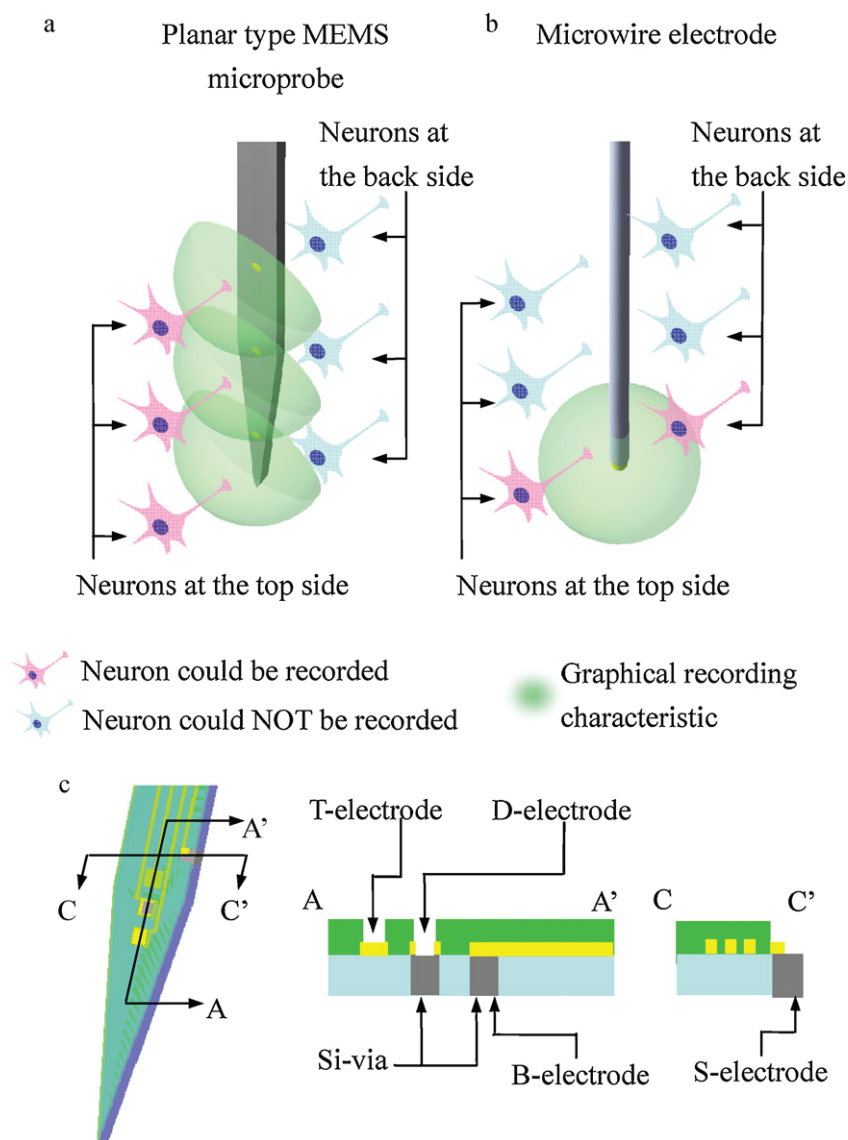


Fig. 1. Schematic illustrations of the recording characteristic of (a) planar type MEMS microprobe, and (b) the microwire electrode. (c) The design concept of the proposed glass microprobe with T-electrode formed by metal film. The B-, D- and S-electrodes are formed by silicon-vias.

cellular potential field. Nevertheless, the measured potential of a microwire electrode with a 3-dimensional surface can average the potential field around the shaft. Thus, microwire electrodes are less sensitive to neuron orientation and can record neural signal around the electrode (Fig. 1b) (Buzsaki, 2004). The performance of planar type MEMS microprobes can be improved if their recording characteristics are made similar to those of a microwire electrode. In this case, planar type MEMS microprobes could provide higher recording density along the shaft and record neurons from all directions (i.e., achieve a 360° recording characteristic).

To address this issue, the distortion effect can be minimized by reducing the shaft size (Drake et al., 1988). However, the shaft size of a planar type MEMS microprobe is restricted by the number and size of electrodes. Thus, researchers have developed various planar type MEMS microprobes with 360° recording characteristics. For example, electrodes can be patterned on both sides of a microprobe using an ultra-thin Si wafer (50 μm or 25 μm) (Du et al., 2009b) and the boron doped Si process, forming top-side and back-side electrodes (Perlin and Wise, 2004). As for polymer-based microprobes, polyimide or parylene-C microprobe with electrodes on

two sides of probe shaft has been demonstrated (Seymour et al., 2011; Stieglitz, 2001; Stieglitz and Gross, 2002). Using a parylene-C based microprobe, Seymour (Seymour et al., 2011) developed an electrode located at the edge of the shaft and having wider recording range.

Researchers have successfully used the glass reflowing process to fabricate glass-based microprobes with embedded silicon (i.e., silicon-vias) (Lee et al., 2010; Lin et al., 2009). Glass has good biocompatibility and has been widely used in many biological applications (Bayliss et al., 1999; Christensen et al., 2007; Lin et al., 2009). This reflowing process can integrate the low resistance silicon structure into the glass substrate to provide versatile functions for microprobe assembly (Lee et al., 2010). Using the glass reflowing process, this study integrates the low resistance silicon structure with the glass shaft to create an electrode material. Thus, a top-side electrode, back-side electrode, double-side electrode, and sidewall electrode can be implemented using the same process. It is easy to fabricate, distribute, and integrate these four types of electrodes on a glass probe. Because these electrodes have different recording characteristics, they can be used in different neural applications in the future.

2. Materials and methods

This section describes the design concept of utilizing silicon as an electrode material to integrate four types of electrodes on a glass microprobe. Specifically, this section describes the fabrication process and experimental method.

2.1. The design of four types of electrodes

This study designs and implements a microprobe with four different electrodes to record neurons around the probe shaft. A metal layer was employed to fabricate the conventional top-side electrode (T-electrode), and the silicon-vias were exploited to realize the other three sensing electrodes. The silicon-via electrodes were fabricated inside the glass based probe shaft using the glass reflow processes (Lee et al., 2010; Lin et al., 2009). As depicted in the AA' cross section of Fig. 1c, the silicon-vias formed the back-side electrode (B-electrode) and double-side electrode (D-electrode). The silicon-via of B-electrode was designed to only be exposed at the back-side of shaft, while the top-side of shaft was covered with insulation parylene-C layer. Thus, the T-electrode mainly records neural signals from the top-side of shaft, whereas the B-electrode mainly records neural signals from the back-side of shaft. On the other hand, the silicon-via of D-electrode is exposed at both sides of shaft, and the D-electrode can record neural signals from both the top-side and the back-side of shaft. Thus, the neural signal amplitude measured by the D-electrode is the average potential of signals recorded from both sides (Perlin and Wise, 2004). As a result, the recorded amplitude of the D-electrode is less sensitive to neuron orientation because it records the average signals.

As indicated in the CC' cross section of Fig. 1c, placing the silicon-via at the edge of glass probe shaft forms a sidewall electrode (S-electrode). Thus, the S-electrode has a 3-dimensional recording surface consisting of the top-side surface, the back-side surface, and the sidewall surface. This 3D electrode surface arrangement is similar to the microwire electrode depicted in Fig. 1b. The silicon via of a D-electrode is embedded within the glass shaft, whereas the silicon via of S-electrode is arranged at the edge of the shaft. Thus, the recording characteristics of S-electrode are less affected by the shielding effect of the shaft (Moffitt and McIntyre, 2005; Seymour and Kipke, 2007; Seymour et al., 2011), and can interact with neurons surrounding the shaft.

2.2. Fabrication process

This study uses the process technology by (Lee et al., 2010; Lin et al., 2009) to implement the proposed microprobe. Firstly, a silicon mold was defined by a two-step deep reactive ion etching (DRIE) process (Figure S1a). After Si-glass anodic bonding, the glass was reflowed into the silicon mold (Figure S1b and c). A lapping process was employed to flatten the substrate surface and expose the silicon electrode (Figure S1d). The metal (Cr/Au) was patterned to define the metal routings and electrodes. A parylene layer was deposited and patterned to define the openings for the front-side electrodes and wire bond pads (Figure S1e and f). This process formed four types of electrodes. Finally, the DRIE processes in Figure S1g and h were used to release the glass microprobe from the silicon substrate.

2.3. In vitro recording characteristic setup and measurement

Figure S2 illustrates the in vitro setup used in this study. A micromanipulator with 10 μm resolution was used to fine-tune the position of the tested microprobe and a tungsten electrode. A function generator delivered a 1 kHz sine-wave voltage (V_{stim}) through the tungsten electrode from the top-side (t), back-side (b), and side-

wall (s) of the probe shaft at a distance d ranging from 40 μm to 160 μm . The tested electrode was connected to an amplifier with 1000 \times gain to record the sine-wave signal delivered by the tungsten electrode. Two separate ground electrodes were employed for voltage recording (R_{gnd}) and voltage delivery (S_{gnd}). Thus, the measurement result was less affected by the impedance of ground electrode (Logothetis et al., 2007). The amplified signal was digitalized and processed using software developed by Brain Research Center, National Tsing Hua University, Taiwan. Under the same conditions (i.e., distance d and stimulating voltage V_{stim}), the number R_{ij} was used to evaluate the recording characteristic of a specific electrode. R_{ij} is the ratio of signal amplitudes recorded from two different positions i and j . For example, a specific electrode first records a signal with amplitude A_t when the tungsten is stimulated from its top-side (t); and then records a signal with amplitude A_b when the tungsten is stimulated from its back-side (b). Thus R_{tb} represents the signal ratio of A_t/A_b . When $R_{ij} \approx 1$, the electrode has the same recording sensitivity for both positions. When $R_{ij} > 1$, the electrode has higher recording sensitivity at position i , and vice versa.

2.4. Crayfish action potential measurement

An adult crayfish was first chilled in cold water, and the head and throax segment were removed. The abdominal segment of the crayfish was dissected to expose the ventral nerve cord. The nerve cord was pinned dorsal side up on a Petri dish and immersed in crayfish saline (Van Harreveld, 1936). The abdominal nerve cord has six segments and each segment has four giant nerves (two lateral giant (LG) and two medial giant (MG)) on the dorsal side. Figure S3 illustrates the experiment setup. A twisted silver wire (stimulator) was placed on the 3rd abdominal segment of the nerve cord to stimulate the nerve and generate action potentials. To record the action potential, the electrode was gently contacted to the 5th LG. During the recording, the stimulation voltage gradually increased (0.1 V/step) to achieve the threshold voltage of the nerve. Thus, an all-or-none behavior of the action potential could be observed, confirming that the recorded signal was the action potential instead of an artifact signal. Fig. 2 shows that the electrodes were contacted to the LG in three different orientations (i.e., top-side contact, sidewall contact, and back-side contact) to evaluate the recording characteristics of each electrode.

2.5. Rat brain action potential measurement

To record the action potential inside a rat brain, a male rat (Sprague Dawley) weighing approximately 250 g was first anesthetized with pentobarbital (intraperitoneal injection, 50 mg/kg), and secured on the stereotaxic frame. The skull and dura on the left M1 region were removed to expose the brain tissue without damaging blood vessels. The packaged microprobe was mounted on a hydraulic micromanipulator (NARISHIGE, MHW-4) and gradually inserted into the brain. The recorded signal was amplified (1000 \times) and monitored by an oscilloscope and a speaker. The amplified signal was digitalized and then filtered by a band pass filter with frequency range from 100 Hz to 10 kHz to reduce the noise.

3. Experiments and results

This section presents the fabrication results of the glass microprobe with silicon-via electrodes. In vitro and in vivo experiments were performed to evaluate the recording characteristics of the fabricated electrodes.

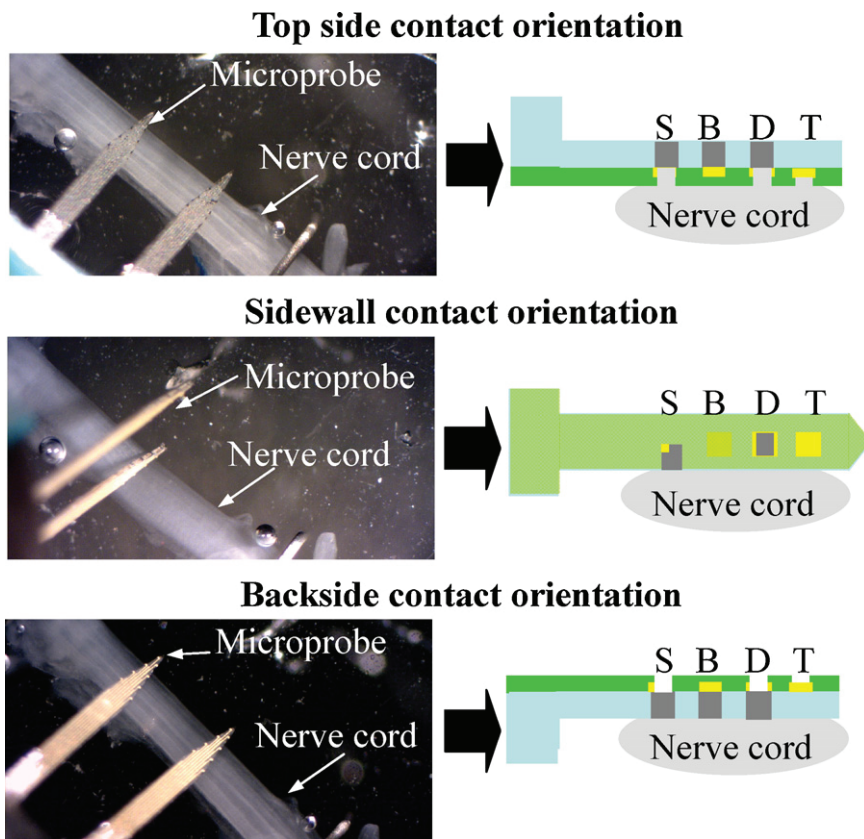


Fig. 2. The crayfish nerve cord recording tests for three different contact orientations: top-side contact orientation, sidewall contact orientation and backside contact orientation. (Illustrations on the right side show the contact between electrodes and nerve cord.)

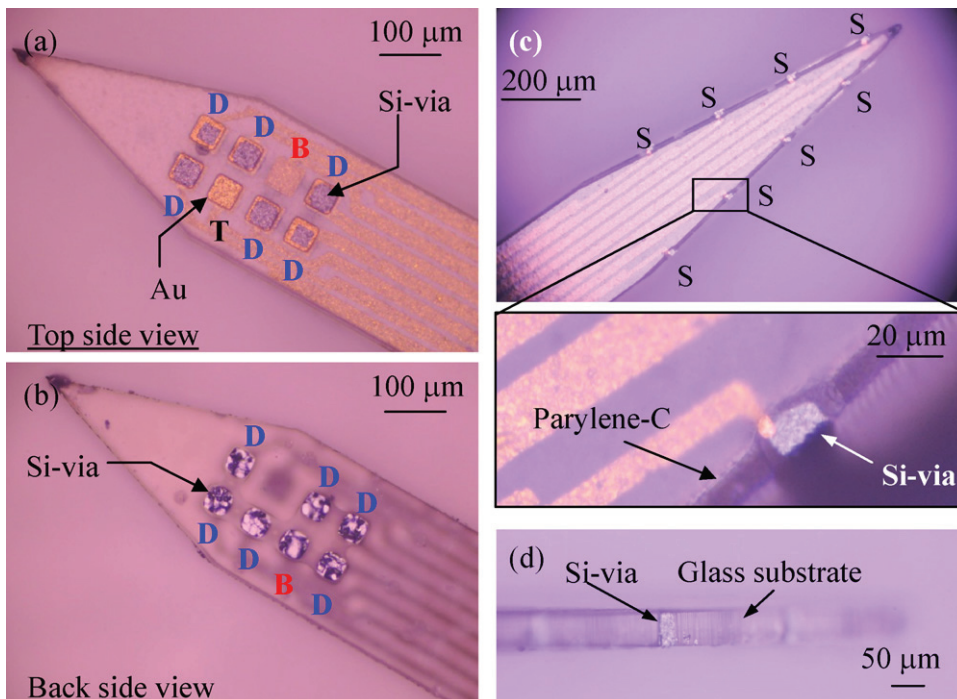


Fig. 3. The fabrication results of the microprobe with T-, B-, D- and S-electrode. (a) and (b) show the T-, B-, and D-electrode are in a cluster arrangement on a transparent glass shaft, (a) the top side view, and (b) the back-side view. (c) and (d) show the fabrication results of the microprobe with S-electrode, (c) the arrangement of eight S-electrodes on microprobe and an enlarged top-side view showing the structure of S-electrode, and (d) the side view shows the sidewall structure of S-electrode.

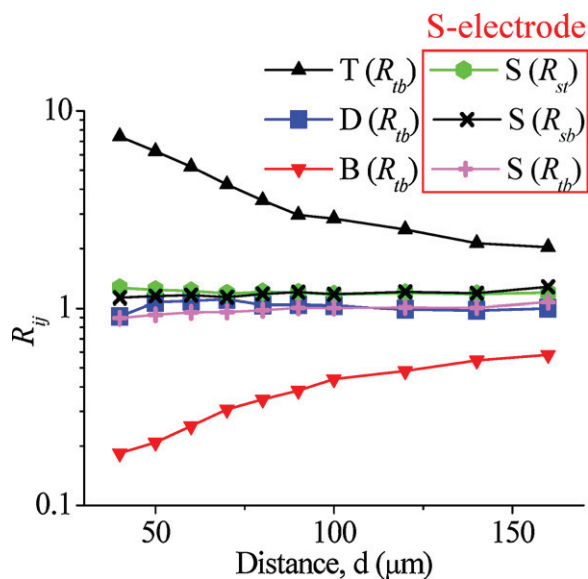


Fig. 4. The experiment results of the in vitro experiment.

3.1. Fabrication results and impedance measurement

Fig. 3 shows the typical fabrication results for four types of electrodes: T-, B-, D-, and S-electrodes. Fig. 3a shows the T-electrode (the conventional planar type MEMS microprobe electrode) formed with only Au film on the top-side of shaft. The D-electrode and B-electrode consisted of silicon-via, and appear in the top-side and back-side micrographs in Fig. 3a and b. The top-side of B-electrode was covered with insulation parylene-C, causing a blurred image in Fig. 3a. Fig. 3c and d show typical fabricated microprobes with S-electrodes. Eight S-electrodes were distributed along the edge of probe shaft. The zoomed-in and side-view micrographs in Fig. 3c and d clearly depict the low resistance silicon-via embedded in the sidewall of glass probe as S-electrode. Figure S4 shows more fabrication results of the microprobes and other arrangement of electrodes.

3.2. Recording characteristic of the electrode (in vitro)

The proposed microprobe was implanted in the rat brain to record neural signals. However, it is difficult to determine the exact position between the electrode and the recorded neurons, which in turn makes it difficult to evaluate the recording characteristic of the electrode. An in vitro experiment was therefore employed to evaluate the recording characteristic with a predetermined distance and location between the voltage source (tungsten electrode) and the tested electrode (T-, D-, B- and S-electrode). The experiment results in Fig. 4 indicate that the R_{tb} value of T-electrode is larger than 1 when d ranges from 40 μm to 160 μm , and reaches its maximum R_{tb} at $d = 40 \mu\text{m}$ (7.41). Moreover, the B-electrode has $R_{tb} < 1$ and has a minimum R_{tb} at $d = 40 \mu\text{m}$ (0.18). This is because the signal recorded by the T-electrode has a larger amplitude, as the tungsten electrode delivers an excitation from the top-side, and the amplitude of recorded signal declines as the stimulating distance (d) increases. When tungsten electrode delivers excitation from the back-side, the signal recorded by the T-electrode is small and its amplitude is relatively insensitive to the stimulation distance d . However, the B-electrode is more sensitive to the excitation of tungsten electrode delivered from the back-side of the shaft. This experiment also shows that the shaft shields the excitation signal when the tested electrode does not directly face the tungsten probe. Therefore, it is difficult for the T-electrode (B-electrode) to record

neurons from the back-side (top-side) of the probe, even when the neurons are very close the shaft. This leads to the recording characteristics in Fig. 1a.

The measurement results in Fig. 4 show that the recording behavior of D-electrode and S-electrode is unlike that of the T-electrode and B-electrode. The D-electrode has $R_{tb} \approx 1$ at different stimulating distance d . As the tungsten probe delivers electrical excitations from the top side and back-side of the shaft (at a specific stimulating distance), the signal amplitudes recorded by the D-electrode are similar. Thus, the D-electrode has an equal recording sensitivity for neurons located at the top-side and back-side of the probe shaft. Moreover, the S-electrode has R_{tb} , R_{sb} , and $R_{st} \approx 1$, which indicates that the S-electrode has equal recording sensitivity for neurons located at top-side, back-side, and sidewall of the probe shaft. In short, the recording characteristic of D- and S-electrodes is similar to the microwire electrode (Fig. 1b). However, unlike the tip electrode on microwire, the proposed D- and S-electrodes can be arbitrarily arranged along the probe shaft using the processes in Figure S1.

3.3. Recording characteristic of the electrode (in vivo)

This study employs in vivo experiments to test the fabricated electrode in real neural systems. The following in vivo experiments were performed on crayfish nerve cord and rat brain. The crayfish nerve cord provides a simplified neural system to investigate the recording characteristics of fabricated electrode, while the rat brain provides an actual biological environment for the fabricated electrode.

3.3.1. Crayfish action potential measurement

Fig. 5 shows the typical action potential recorded from crayfish. All four types of electrodes could successfully record action potential with a good signal to noise ratio from the crayfish nerve cord. Since LG cell are visible under a stereo microscope, the contact condition between the tested electrode and LG cell could be controlled during the experiment. Moreover, the conditions (such as the action potential current flow through the ion channel and the membrane property) of the LG cell remained constant when the tested electrode was placed in different contact orientations. Thus, the extracellular amplitude of LG action potential was constant, and the recording characteristic of specific electrode could be evaluated by the recorded action potential amplitude at different contact orientations. For the T-electrode and B-electrode, the action potential amplitudes recorded from top-side and back-side orientation, respectively, were significantly different (Fig. 5). The action potential recorded by the T-electrode had a larger amplitude for the top-side contact condition, whereas that recorded by B-electrode had a larger amplitude for the back-side contact condition.

Fig. 5 also shows the results recorded by the D- and S-electrodes. The D- and S-electrodes have multiple recording surfaces. Though the experiments in this study only allows one recording surface to touch the LG neuron for each particular contact orientation, the neural signal amplitude recorded by the D- and S-electrode is the average value of signals measured from each recording surface, as discussed in Section 2.1. This is why the measurement results for D-electrode in Fig. 5 show that the action potential amplitudes measured from the top-side and back-side contact conditions were similar. Similarly, the measurement results for S-electrode in Fig. 5 show that, the action potential amplitudes respectively recorded from three different contact orientations in Fig. 2 were similar. Moreover, for the measurements of top-side contact condition, the action potential amplitude recorded from the D- and S-electrodes was smaller than that recorded from the T-electrode. For the measurements of back-side contact condition, the action potential amplitude recorded from the D- and S-electrodes was

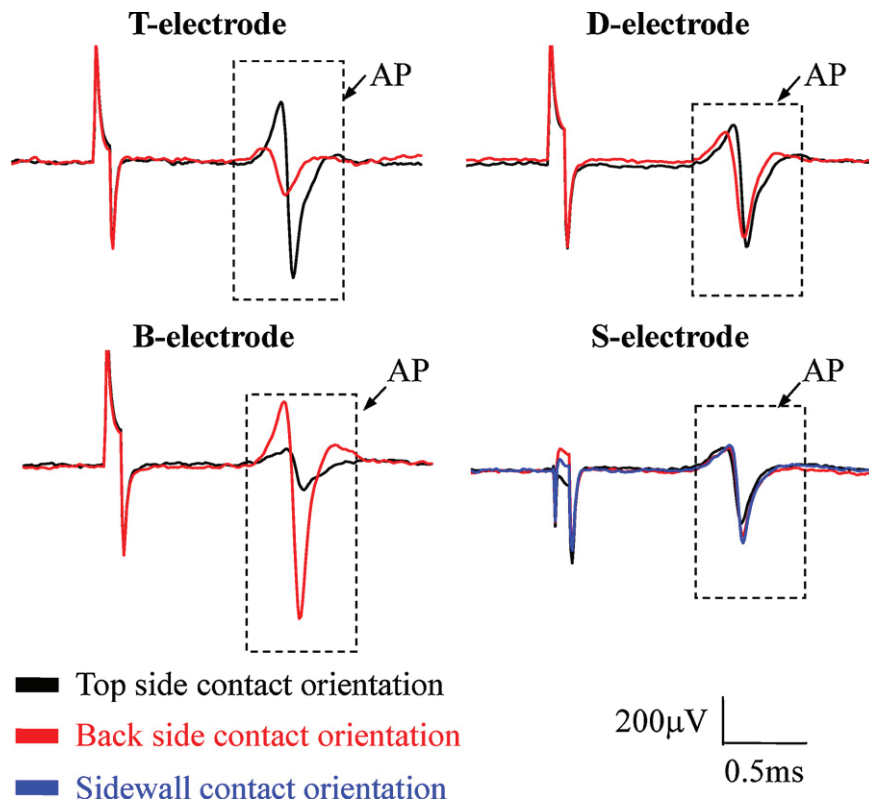


Fig. 5. The action potentials (AP) recorded from T-, B-, D- and S-electrode at different contact orientations during the crayfish nerve cord tests.

smaller than that recorded from the B-electrode. These characteristics are due to the average effect, and agree with the discussion in Section 2.1. In summary, the in vivo experiment results agree well with the in vitro test results in Section 3.2. The T-electrode and B-electrode were more sensitive to the voltage source generated from the top-side and back-side of probe shaft, while the signal amplitude recorded by the D- and S-electrode was less sensitive to the location of the voltage source.

3.3.2. Rat brain action potential measurement

The recording condition in the crayfish was different from the recording condition in the rat brain. For example, the size of the neuron cell and the contact condition between the electrode and neurons are different. To investigate the performance of the fabricated electrode in brain tissue, the microprobe shown in Fig. 3a and b was implanted into the rat brain to record the action potential simultaneously from four electrodes (one T-electrode, one B-electrode, and two D-electrodes). The recording results in Fig. 6 demonstrate that the T-, B-, D- and S-electrodes could successfully record the action potential from neurons inside the rat brain.

As shown in the selected trace in Fig. 6a, the action potentials recorded by T-electrode were not recorded by the B-electrode, and vice versa. In this experiment, the distance and orientation of neurons to the electrodes influenced the action potential amplitude recorded by the electrode. However, the position of neurons during the measurement was unknown. Nevertheless, the experimental results in Sections 3.2 and 3.3.1 show the T- and B-electrode have different sensitivities to neurons at different sides of microprobe shaft. Thus, the results in Fig. 6a could be interpreted as different groups of neurons from the top-side and back-side of the shaft recorded by T- and B-electrodes, respectively. Moreover, the action potential recorded by the D-electrode (D1 and D2) was coincident with the action potential recorded by the T- and B-electrodes in time, as indicated by marks I–VII in Fig. 6a.

The action potentials recorded by D1 and D2 suggest that a D-electrode can record neurons at both sides of the probe shaft. Moreover, the recorded trace of D1 and D2 are different (Fig. 6a). The amplitude of the recorded extracellular potential varied with the distance between electrode and neurons. The 100 μm center-to-center distance between D1 and D2 electrodes could lead to different distances between electrodes and neurons, and further cause the difference of recorded signals by these two electrodes. In this experiment, the S-electrode typically has a better signal to noise ratio (SNR) than the D-electrode. As shown in Fig. 6b, the SNR of the S-electrode is 12.7–26.3 (with an average SNR of 19.9), while in Fig. 6a, the SNR of D-electrodes are 6.5–16.26 (with an average SNR of 11.38). The SNR is defined as the ratio of peak-to-peak value of action potential to the root-mean-square value of the noise. This characteristic could result from a smaller shielding effect of the S-electrode (Drake et al., 1988; Seymour and Kipke, 2007).

4. Discussion

Planar type MEMS microprobes can generally arrange multiple T-electrodes on the probe shaft to increase the recording density. However, as demonstrated in this study, the shaft shields the neural signal from the back-side of microprobe, limiting the recording range of the T-electrode. This study develops B-electrodes that could record neural signals from the back-side of the probe shaft. The proposed microprobe, with integrated T-electrode and B-electrodes, can distinguish neuron signals from both sides of the probe shaft. This arrangement can extend the 2-dimensional neurons localization to 3-dimensional localization (Bartho et al., 2004; Du et al., 2009a), and therefore reveal more details about the neuron wiring and distribution in the brain. The in vitro and in vivo measurement results in Figs. 4–6 show that the D-electrode can simultaneously record neurons from two sides of the microprobe. This study also demonstrates the recording capability of the

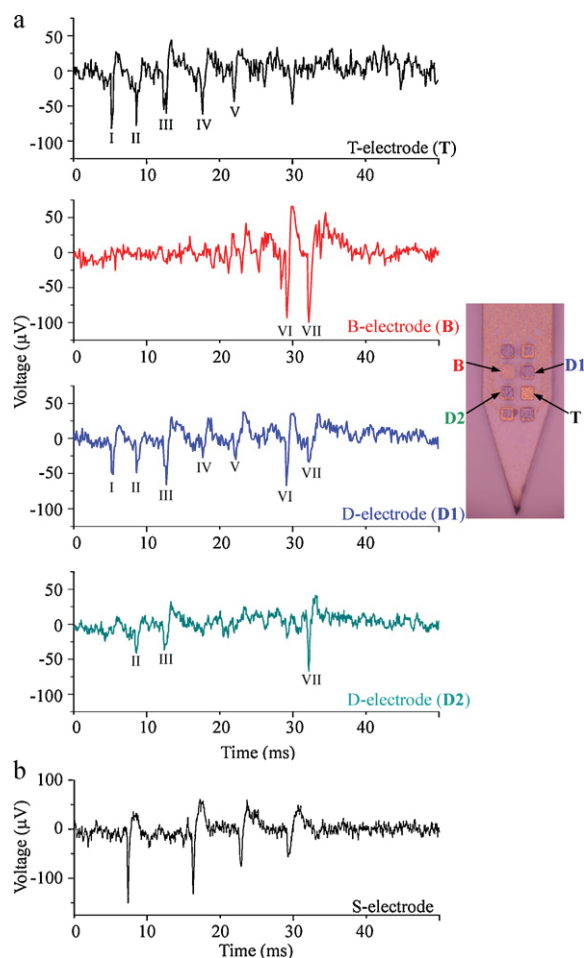


Fig. 6. The action potentials recorded in rat's brain using different microprobes, (a) the action potentials simultaneously recorded from the four electrodes (one T-electrode, one B-electrode, and two D-electrodes) on the microprobe shown in Fig. 3a and b, and (b) the action potential recorded from one S-electrode on the microprobe shown in Fig. 3c and d.

S-electrode from three sides of the probe shaft through in vitro and crayfish experiments (Figs. 4 and 5). In summary, a spherical recording range can be achieved by single S- or D-electrodes or combining a pair of T- and B-electrode on the microprobe. Although the integration of T- and B-electrodes also can achieve a spherical recording range, an additional signal processing unit (i.e. amplifier, AD/DA converter) is required to process the data. The trade-off of using S- and D-electrode is losing the spatial discrimination from the top and back-sides of probe shaft. In this regard, the S- and D-electrode is more suitable for chronic applications, which require greater recording density than spatial discrimination.

The experiments in this study successfully fabricated and integrated four types of electrodes (T-, B-, D- and S-electrodes) using the glass reflowing process. The arrangement of different types of electrodes could be easily achieved by fabrication processes through the patterning of metal layer, silicon-vias, and insulation parylene-C layer. Compared to previous methods, which only support T- and B-electrodes (Du et al., 2009b; Stieglitz, 2001; Stieglitz and Gross, 2002), the presented glass reflowing process implement four types of electrodes and can provide more flexible electrode arrangement. Multi-type thin metal electrodes have been respectively fabricated in thin Si substrate (Perlin and Wise, 2004) and polymer substrate (Seymour et al., 2011). Thus, the probe stiffness to prevent bucking or break during the insertion is a critical concern for these two designs. In comparison, the proposed silicon-

via structure enables the implementation of a thick electrode on a thick glass shaft. The thickness of silicon-via and shaft can be easily and simultaneously defined by the DRIE and glass molding process (Figure S1). Thus, it is easy for the presented microprobe to adjust the thickness and stiffness of the shaft for different applications.

Single crystal silicon (SCS) has been commonly used as a structural material in MEMS microprobes (Bhandari et al., 2008; Blanche et al., 2005; Du et al., 2009b; Herwik et al., 2009; Norlin et al., 2002; Perlin and Wise, 2004). This paper first demonstrates the use of SCS as an electrode material. As Figure S5 shows, an SCS electrode (B-electrode) has a higher impedance ($3.0\text{ M}\Omega @ 1\text{ kHz}$) than a gold electrode (T-electrode, $1.48\text{ M}\Omega @ 1\text{ kHz}$). Thus, the silicon electrode produces greater thermal noise. Nevertheless, the major noise source contributed to electrode is the background neural noise in the biological environment, instead of thermal noise from the electrode (Cogan, 2008; Ward et al., 2009). Figs. 5 and 6 show that the recording results from crayfish nerve cord and rat brain indicate the recording ability of silicon electrode is comparable to the gold electrode (T-electrode). Thus, the silicon electrode is compatible with various recording applications. For stimulating application, such as the deep brain stimulation (DBS), the impedance of the silicon electrode need to be further decreased to effectively stimulate the neurons. Materials such as iridium oxide, carbon nanotube, or poly(3, 4-ethylenedioxythiophene) has been extensively used to decrease the impedance of conventional electrode (Hsu et al., 2010; Keefer et al., 2008; Meyer et al., 2002; Yang and Martin, 2004a,b). It is possible to selectively deposit materials such as electroplated poly(3, 4-ethylenedioxythiophene) for the proposed silicon electrode to decrease its impedance in the future. Thus, the glass microprobe could be further used in stimulation applications.

5. Conclusion

This study successfully employs a glass reflowing process to implement and integrate silicon electrodes into a glass microprobe. Through the patterning and arrangement of the metal layer, silicon-vias, and the insulation parylene-C layer, four types of electrodes can be arbitrary distributed on the probe shaft. In-vitro experiments and crayfish nerve cord recording experiments indicate that the D- and S-electrodes are less sensitive to the neuron locations around the probe shaft, whereas the T- and B-electrodes are relatively sensitive to the neuron locations. The action potentials recorded from crayfish nerve cord and rat brain show that the recording ability of the silicon electrode is comparable to that of a gold electrode (T-electrode). The rat brain experiment further demonstrates that the D-electrode can simultaneously record the action potentials respectively detected by the T-electrode and B-electrode. In summary, the proposed silicon electrode provides a spherical recording range on the planar type MEMS microprobe. The proposed technique can easily integrate and arrange metal and silicon-via electrodes on a glass microprobe to meet the various requirements of acute or chronic recording applications.

Acknowledgements

This research was sponsored in part by the NSC of Taiwan under grant no. NSC-99-2627-E-007-002. The authors would like to thank the Nano Facility Center of National Tsing Hua U., and the NEMS Research Center of National Taiwan U. for providing the fabrication facilities. The authors also would like to thank Mr. Yung-Chan Chen, and Prof. Hsin Chen of National Tsing Hua U. for providing the impedance measurement.

Appendix A. Supplementary data

Supplementary data associated with this article can be found in the online version, at doi:10.1016/j.bios.2011.05.037.

References

- Bartho, P., Hirase, H., Monconduit, L., Zugaro, M., Harris, K., Buzsaki, G., 2004. *J. Neurophysiol.* 92, 600–608.
- Bayliss, S.C., Buckberry, L.D., Fletcher, I., Tobin, M.J., 1999. *Sens. Actuators A-Phys.* 74, 139–142.
- Bhandari, R., Negi, S., Rieth, L., Normann, R.A., Solzbacher, F., 2008. *Sens. Actuators A-Phys.* 145, 123–130.
- Bhandari, R., Negi, S., Rieth, L., Normann, R.A., Solzbacher, F., 2009. *J. Micromech. Microeng.* 19, 035004.
- Blanche, T.J., Spacek, M.A., Hetke, J.F., Swindale, N.V., 2005. *J. Neurophysiol.* 93, 2987–3000.
- Buzsaki, G., 2004. *Nat. Neurosci.* 7, 446–451.
- Campbell, P.K., Jones, K.E., Huber, R.J., Horch, K.W., Normann, R.A., 1991. *IEEE Trans. Biomed. Eng.* 38, 758–768.
- Christensen, T.B., Pedersen, C.M., Grondahl, K.G., Jensen, T.G., Sekulovic, A., Bang, D.D., Wolff, A., 2007. *J. Micromech. Microeng.* 17, 1527–1532.
- Cogan, S.F., 2008. *Annu. Rev. Biomed. Eng.* 10, 275–309.
- Drake, K.L., Wise, K.D., Farraye, J., Anderson, D.J., BeMent, S.L., 1988. *IEEE Trans. Biomed. Eng.* 35, 719–732.
- Du, J., Riedel-Kruse, I.H., Nawroth, J.C., Roukes, M.L., Laurent, G., Masmanidis, S.C., 2009a. *J. Neurophysiol.* 101, 1671–1678.
- Du, J., Roukes, M.L., Masmanidis, S.C., 2009b. *J. Micromech. Microeng.* 19, 075008.
- Herwik, S., Kisban, S., Aarts, A.A.A., Seidl, K., Girardeau, G., Benchenane, K., Zugaro, M.B., Wiener, S.I., Paul, O., Neves, H.P., 2009. *J. Micromech. Microeng.* 19, 074008.
- Hsu, H.L., Teng, I.J., Chen, Y.C., Hsu, W.L., Lee, Y.T., Yen, S.J., Su, H.C., Yeh, S.R., Chen, H., Yew, T.R., 2010. *Adv. Mater.* 22, 2177–2181.
- Keefer, E.W., Botterman, B.R., Romero, M.L., Rossi, A.F., Gross, G.W., 2008. *Nat. Nanotechnol.* 3, 434–439.
- Lee, Y.T., Lin, C.W., Lin, C.M., Yeh, S.R., Chang, Y.C., Fang, W., 2010. *J. Micromech. Microeng.* 20, 025014.
- Lin, C.W., Lee, Y.T., Chang, C.W., Hsu, W.L., Chang, Y.C., Fang, W., 2009. *Biosens. Bioelectron.* 25, 475–481.
- Logothetis, N.K., Kayser, C., Oeltermann, A., 2007. *Neuron* 55, 809–823.
- McCreery, D., Lossinsky, A., Pikov, V., Liu, X., 2006. *IEEE Trans. Biomed. Eng.* 53, 726–737.
- Meyer, R.D., Cogan, S.F., Nguyen, T.H., Rauh, R.D., 2002. *Transactions on Neural Systems and Rehabilitation Engineering IEEE*, vol. 9, pp. 2–11.
- Moffitt, M.A., McIntyre, C.C., 2005. *Clin. Neurophysiol.* 116, 2240–2250.
- Musallam, S., Bak, M.J., Troyk, P.R., Andersen, R.A., 2007. *J. Neurosci. Methods* 160, 122–127.
- Nicolelis, M.A.L., Lebedev, M.A., 2009. *Nat. Rev. Neurosci.* 10, 530–540.
- Norlin, P., Kindlundh, M., Mouroux, A., Yoshida, K., Hofmann, U.G., 2002. *J. Micromech. Microeng.* 12, 414–419.
- Perlin, G.E., Wise, K.D., 2004. *Proceedings of the 26th Annual International Conference of the IEEE EMBS*, pp. 2002–2005.
- Rall, W., 1962. *Biophys. J.* 2, 145–167.
- Seymour, J.P., Kipke, D.R., 2007. *Biomaterials* 28, 3594–3607.
- Seymour, J.P., Langhals, N.B., Anderson, D.J., Kipke, D.R., 2011. *Biomed. Microdev.* 13, 441–451.
- Stieglitz, T., 2001. *Sens. Actuators A-Phys.* 90, 203–211.
- Stieglitz, T., Gross, M., 2002. *Sens. Actuators B-Chem.* 83, 8–14.
- Van Harreveld, A., 1936. *Proc. Soc. Exp. Biol. Med.* 34, 428–432.
- Velliste, M., Perel, S., Spalding, M.C., Whitford, A.S., Schwartz, A.B., 2008. *Nature* 453, 1098–1101.
- Ward, M.P., Rajdev, P., Ellison, C., Irazoqui, P.P., 2009. *Brain Res.* 1282, 183–200.
- Yang, J., Martin, D.C., 2004a. *Sens. Actuators B-Chem.* 101, 133–142.
- Yang, J., Martin, D.C., 2004b. *Sens. Actuators A-Phys.* 113, 204–211.